On the PAPR of Discrete Zak Transform Based OTFS Modulation

Vineetha Yogesh, Anagha V, Sandesh Rao Mattu, and A. Chockalingam
Department of ECE, Indian Institute of Science, Bangalore

***Abstract*—Recently, Zak transform based orthogonal time frequency space (OTFS) waveform has generated new research interest owing to its better robustness to large channel spreads compared to that of the widely researched OTFS waveform based on inverse symplectic finite Fourier transform (ISFFT) and Heisenberg transform (HT). In this paper, we investigate the peak-to-average power ratio (PAPR) characteristics of discrete Zak transform based OTFS (DZT-OTFS), which has not been reported. We derive an upper bound on the PAPR of DZT-OTFS waveform for general transmit pulse shapes and a tighter upper bound for rectangular pulse, using Cauchy-Schwartz inequality. The PAPR upper bound for DZT-OTFS and two-step OTFS (based on ISFFT and HT) are shown to be the same for rectangular pulse, and hence the PAPR of DZT-OTFS with rectangular transmit pulse shape grows linearly in the number of Doppler bins. With non-rectangular transmit pulse, the results on complementary cumulative distribution function (CCDF) of PAPR show that DZT-OTFS can have better PAPR characteristics compared to that of two-step OTFS.**

***Index Terms*—Peak-to-average power, Zak transform, OTFS modulation, delay-Doppler domain, two-step OTFS.**

I. Introduction

To cater to the evolving requirements of next generation wireless systems, it is important to achieve reliable communication in high-Doppler channels. While traditional communications schemes like orthogonal frequency division multiplexing (OFDM) can work well in frequency selective channels, they fail under time selectivity caused by high Doppler spreads. It has been shown that orthogonal time frequency space (OTFS) modulation converts a high-Doppler channel to an almost time-invariant channel by virtue of multiplexing data symbols and viewing the channel response in the delay-Doppler (DD) domain [1], [2]. Most research on OTFS so far uses a two-step transform approach, where the information symbols multiplexed in the DD domain are converted to time domain for transmission in two steps, viz., DD domain to time-frequency (TF) domain conversion using inverse symplectic finite Fourier transform (ISFFT) followed by TF domain to time domain conversion using Heisenberg transform. In more recent research, a direct one-step transform approach for realizing OTFS, namely, direct conversion of DD domain symbols to time domain at the transmitter and vice versa at the receiver using Zak transform framework [3], has been shown to be more robust to large channel spreads compared to the two-step transform approach [4]-[7]. We focus on the Zak transform approach to OTFS in this paper.

This work was supported in part by the J. C. Bose National Fellowship, Department of Science and Technology, Government of India. The first author would like to thank the Prime Minister's Research Fellowship, Ministry of Education, Government of India for the support.

We provide a summary of recent research on Zak transform based OTFS as follows. In [4], Zak transform based OTFS has been derived from first principles, and it has been shown that the spectral efficiency performance of the Zak approach remains invariant to user velocity. The work in [5] has considered a system with two-step OTFS at the transmitter and showed that using a single-step Zak based OTFS receiver is more robust to high Dopplers than using a two-step OTFS receiver. It also showed that Zak based time domain to DD domain transformation (and vice versa) has a lower complexity compared to two-step transformation. The recently reported works in [6], [7] delve on the fundamental features of Zak based OTFS that are instrumental for its superior performance in high-Doppler channels compared to two-step OTFS and OFDM. It identifies predictability of the input-output relation and non-fading attributes in Zak based OTFS as key for the robustness of the Zak based approach to OTFS. This has created interest and opportunities for new research in Zak based OTFS. Recently, the authors in [8] have derived the DD domain input-output relation for a discrete Zak transform (DZT) based OTFS (DZT-OTFS) system. Subsequently, the works in [9], [10] have reported the bit error rate (BER) performance of DZT-OTFS.

In a related context, index modulation is a physical layer technique in which indexing of transmit entities (e.g., transmit antennas, subcarriers) is used to convey information bits [16]. Indexing of DD bins in OTFS has been of interest because of its better resilience to Doppler spreads and improved diversity performance [17], [18]. In index modulated OTFS, inactive DD bins are filled with zeros which can lead to better PAPR performance [18]. Owing to the BER performance and complexity advantages of Zak based OTFS, it is of interest to study and characterize its peak-to-average power ratio (PAPR) performance, which has not been reported. Consequently, in this paper, we analyze the PAPR characteristics of DZT-OTFS without and with DD domain indexing. A summary of the work and results reported in this paper is as follows.

- We derive an upper bound on the PAPR of DZT-OTFS for general transmit pulse shapes and a tighter bound for rectangular pulse, using Cauchy-Schwartz inequality.
- For rectangular pulse, the PAPR upper bound for DZT-OTFS and two-step OTFS based on ISFFT and Heisenberg transform (derived in [11]) are shown to be the same.
- For non-rectangular pulses, results on the complementary cumulative distribution function (CCDF) of the PAPR show that DZT-OTFS can have better PAPR characteristics compared to that of two-step OTFS. Results with both Nyquist sampling and oversampling are presented.

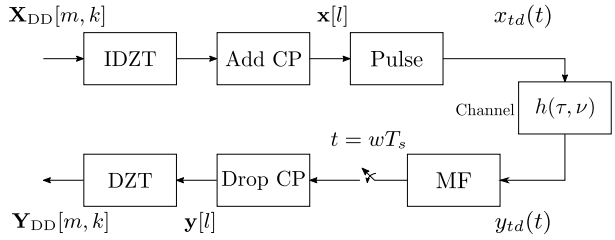

Fig. 1. Block diagram of DZT-OTFS system.

- Indexing of DD bins along Doppler axis is shown to improve the PAPR of DZT-OTFS. Also, for non-rectangular pulse, DZT-OTFS with Doppler indexing has better PAPR compared to two-step OTFS with Doppler indexing.

II. DZT-OTFS SYSTEM MODEL

Figure 1 shows the block diagram of the DZT-OTFS system. At the transmitter, KL information symbols in the DD domain are chosen from a modulation alphabet $\mathbb{A}$, denoted by $\mathbf{X}_{\mathrm{DD}}[m,k] \in \mathbb{A}$, $0 \leq m \leq L-1$, $0 \leq k \leq K-1$, where K and L are the number of Doppler and delay bins, respectively. Resolution along the delay axis is given by $\Delta\tau = T_s$, and the resolution along the Doppler axis is given by $\Delta\nu = \frac{1}{KLT_s}$, where $T_s = 1/B$ is the symbol duration and B is the bandwidth of the system. These information symbols in the DD domain are converted to time-domain by using the inverse discrete Zak transform (IDZT). After passing the symbols through a parallel-to-serial converter, a KL-dimensional vector in time domain is obtained. A cyclic prefix (CP) of length L_{CP} is added to the time domain sequence in order to reduce inter-frame interference. The resulting sequence is mounted on a transmit pulse ($p_{tx}(t)$) to obtain a continuous-time signal for transmission. This time domain signal is passed through the wireless channel. At the receiver, the received signal is matched filtered using $p^*_{tx}(-t)$ and sampled at $f_s = 1/T_s$, and the CP is discarded. The output is converted back to DD domain using discrete Zak transform (DZT) for signal detection.

A. DZT-OTFS transmit signal

At the transmitter, KL-length time domain sequence is obtained from the information symbols $\mathbf{X}_{\mathrm{DD}}[m,k], 0 \leq m \leq L-1$, $0 \leq k \leq K-1$ using the IDZT operation, given by

$$\mathbf{x}[m+qL] = \frac{1}{\sqrt{K}} \sum_{k=0}^{K-1} \mathbf{X}_{\mathrm{DD}}[m,k] e^{j2\pi \frac{k}{K} q}, \tag{1}$$

where $0 \leq m \leq L-1$ and $0 \leq q \leq K-1$. This time domain sequence is mounted on a transmit pulse, $p_{tx}(t)$ to get the time domain signal, $x_{td}(t)$, as

$$x_{td}(t) = \sum_{l=0}^{KL-1} \mathbf{x}[l] p_{tx}(t - lT_s). \tag{2}$$

We sample $x_{td}(t)$ at the Nyquist sampling rate $f_s = \frac{1}{T_s}$ to obtain the discrete-time representation of the transmitted signal in (2), as

$$x_{td}[w] = \sum_{l=0}^{KL-1} \mathbf{x}[l] p_{tx}[w-l], \tag{3}$$

where $w = 0, 1, \cdots, KL-1$, $x_{td}[w] = x_{td}(wT_s)$ and $p_{tx}[w] = p_{tx}(wT_s)$. For a rectangular pulse, given by

$$p_{tx}(t) = \begin{cases} 1, & 0 \leq t < T_s \\ 0, & \text{otherwise,} \end{cases} \tag{4}$$

(3) simplifies to

$$x_{td}[w] = \mathbf{x}[w]. \tag{5}$$

In the next section, we analyze the PAPR characteristics of DZT-OTFS using the time domain samples in (3).

III. PAPR OF DZT-OTFS

In this section, we analyze the PAPR characteristics of DZT-OTFS. We derive an upper bound on the PAPR of DZT-OTFS using Cauchy-Schwartz inequality. The PAPR of a discrete-time signal $\mathbf{x}[w], w = 0, 1, \cdots, KL-1$ is defined as

$$\mathrm{PAPR} = \frac{\max\limits_{w} \{|\mathbf{x}[w]|^2\}}{P_{avg}}, \tag{6}$$

where

$$P_{avg} = \frac{1}{KL} \left[\sum_{w=0}^{KL-1} \mathbb{E}\{|\mathbf{x}[w]|^2\} \right]. \tag{7}$$

For DZT-OTFS, PAPR is computed using the time domain sequence, $x_{td}[w]$, in (3). The numerator in (6) is evaluated as

$$\max_{w} \{|x_{td}[w]|^2\} = \max_{w} \left\{ \left| \sum_{l=0}^{KL-1} \mathbf{x}[l] p_{tx}[w-l] \right|^2 \right\}. \tag{8}$$

Using Cauchy-Schwartz inequality, (8) can be upper bounded as

$$\max_{w} \{|x_{td}[w]|^2\} \leq \sum_{l=0}^{KL-1} |\mathbf{x}[l]|^2 \max_{w} \left\{ \sum_{l=0}^{KL-1} |p_{tx}[w-l]|^2 \right\}. \tag{9}$$

Defining $B_1 \triangleq \max\limits_{w} \left\{ \sum\limits_{l=0}^{KL-1} |p_{tx}[w-l]|^2 \right\}$ and rewriting $\mathbf{x}[l]$ as $\mathbf{x}[m+qL]$ (from (1)), (9) becomes

$$\max_{w} \{|x_{td}[w]|^2\} \leq \sum_{m=0}^{L-1} \sum_{q=0}^{K-1} |\mathbf{x}[m+qL]|^2 B_1. \tag{10}$$

Substituting for $\mathbf{x}[m+qL]$ from (1), (10) can be written as

$$\max_{w} \{|x_{td}[w]|^2\} \leq \sum_{m=0}^{L-1} \sum_{q=0}^{K-1} \left| \frac{1}{\sqrt{K}} \sum_{k=0}^{K-1} \mathbf{X}_{\mathrm{DD}}[m,k] e^{j2\pi \frac{k}{K} q} \right|^2 B_1. \tag{11}$$

Note that the term $\frac{1}{\sqrt{K}}\sum_{k=0}^{K-1}\mathbf{X}_{\mathrm{DD}}[m,k]e^{j2\pi\frac{k}{K}q}$ is the inverse discrete Fourier transform (IDFT) of the information symbols, $\mathbf{X}_{\mathrm{DD}}[m,k]$ for a given m. Parseval's theorem for a particular m in this case is given by

$$\sum_{q=0}^{K-1}|\mathbf{x}[m+qL]|^2=\sum_{k=0}^{K-1}|\mathbf{X}_{\mathrm{DD}}[m,k]|^2. \tag{12}$$

Applying the theorem to simplify (10), we get

$$\max_{w}\{|x_{td}[w]|^2\}\leq\sum_{m=0}^{L-1}\sum_{k=0}^{K-1}|\mathbf{X}_{\mathrm{DD}}[m,k]|^2B_1. \tag{13}$$

Since each symbol in $\mathbf{X}_{\mathrm{DD}}[m,k]$ is drawn from an alphabet $\mathbb{A}$ (e.g. PSK, QAM), the upper bound on the numerator can be written as

$$\max_{w}\{|x_{td}[w]|^2\}\leq KL\max_{a\in\mathbb{A}}\{|a|^2\}B_1. \tag{14}$$

The denominator in (6), P_{avg}, is evaluated using (3), which yields

$$P_{avg}=\frac{1}{KL}\left[\sum_{w=0}^{KL-1}\mathbb{E}\left\{\left|\sum_{l=0}^{KL-1}\mathbf{x}[l]p_{tx}[w-l]\right|^2\right\}\right]. \tag{15}$$

Since $\mathbf{X}_{\mathrm{DD}}[m,q]$s are information symbols drawn from the modulation alphabet $\mathbb{A}$, they can be considered i.i.d. with zero mean and variance $\sigma_s^2=\mathbb{E}\{|\mathbf{X}_{\mathrm{DD}}[m,q]|^2\}$. Also, because of the transmit signal's Nyquist sampling, the samples $x_{td}[w]$s are mutually uncorrelated. Using the above simplifications, (15) can be written as

$$P_{avg}=\frac{1}{KL}\left[\sum_{w=0}^{KL-1}\sum_{l=0}^{KL-1}\mathbb{E}\{|\mathbf{x}[l]|^2\}|p_{tx}[w-l]|^2\right]. \tag{16}$$

Since the sequence $\mathbf{x}[l]$ is the IDZT of the i.i.d. symbols $\mathbf{X}_{\mathrm{DD}}[m,q]$, it's seen that $\mathbb{E}\{|\mathbf{x}[l]|^2\}=\sigma_s^2$, $0\leq l\leq KL-1$. Thus, (16) can be written as

$$P_{avg}=\frac{\sigma_s^2}{KL}\left[\sum_{w=0}^{KL-1}\sum_{l=0}^{KL-1}|p_{tx}[w-l]|^2\right]. \tag{17}$$

Defining $B_2\triangleq\frac{1}{KL}\left[\sum_{w=0}^{KL-1}\sum_{l=0}^{KL-1}|p_{tx}[w-l]|^2\right]$, (17) becomes

$$P_{avg}=\sigma_s^2B_2. \tag{18}$$

From (6), (14), (18), the PAPR of the DZT-OTFS signal is upper bounded as

$$\mathrm{PAPR}_{\mathrm{dzt}}\leq\frac{KL\max\limits_{a\in\mathbb{A}}\{|a|^2\}B_1}{\sigma_s^2B_2}. \tag{19}$$

For the special case of rectangular pulse, a bound tighter than the one in (19) can be obtained by using the transmitted signal in (5) and applying Cauchy-Schwartz inequality to $|\mathbf{x}[m+qL]|^2$, as described below.

For rectangular transmit pulse, $p_{tx}(t)$ is given by (4). The time domain samples are given by (5), as $x_{td}[w]=\mathbf{x}[w]$. The numerator of the PAPR expression in (6) is evaluated (using (1)) as

$$\max_{m,q}\{|\mathbf{x}[m+qL]|^2\}=\max_{m,q}\left|\frac{1}{\sqrt{K}}\sum_{k=0}^{K-1}\mathbf{X}_{\mathrm{DD}}[m,k]e^{j2\pi\frac{k}{K}q}\right|^2. \tag{20}$$

Using Cauchy-Schwartz inequality, (20) can be written as

$$\max_{m,q}\ \{|\mathbf{x}[m+qL]|^2\}\leq \max_{m,q}\ \left[\frac{1}{K}\sum_{k=0}^{K-1}|\mathbf{X}_{\mathrm{DD}}[m,k]|^2\sum_{k=0}^{K-1}\left|e^{j2\pi\frac{k}{K}q}\right|^2\right]. \tag{21}$$

Noting that the absolute value of the complex exponent is 1 and simplifying, we get

$$\max_{m,q}\{|\mathbf{x}[m+qL]|^2\}\leq\max_{m}\sum_{k=0}^{K-1}|\mathbf{X}_{\mathrm{DD}}[m,k]|^2. \tag{22}$$

Since all the symbols $\mathbf{X}_{\mathrm{DD}}[m,k]\in\mathbb{A}$, we can write

$$\max_{m,q}\ \{|\mathbf{x}[m+qL]|^2\}\leq K\max_{a\in\mathbb{A}}\{|a|^2\}. \tag{23}$$

We evaluate the denominator of PAPR in (6) using the fact that $\mathbb{E}\{|\mathbf{x}[l]|^2\}=\sigma_s^2$, $0\leq l\leq KL-1$ to obtain

$$P_{avg}=\frac{1}{KL}\left[\sum_{w=0}^{KL-1}\mathbb{E}\{|\mathbf{x}[w]|^2\}\right]=\sigma_s^2. \tag{24}$$

Therefore, the upper bound on the PAPR of DZT-OTFS for rectangular transmit pulse is obtained as

$$\mathrm{PAPR}_{\mathrm{dzt,rect}}\leq\frac{K\max\limits_{a\in\mathbb{A}}\{|a|^2\}}{\sigma_s^2}. \tag{25}$$

Remark: We note that the upper bound on the PAPR of two-step OTFS obtained in [11] is

$$\mathrm{PAPR}_{\mathrm{2step}}\leq\frac{N\max\limits_{k,l}\{|x[k,l]|^2\}B_1}{\sigma_a^2B_2}, \tag{26}$$

where k and l are the Doppler and delay indices, respectively, N and M are the number of Doppler and delay bins, respectively, $x[k,l]\in\mathbb{A}$ denotes the information symbol in the DD domain, and $\sigma_a^2=\mathbb{E}\{|\mathbf{x}[k,l]|^2\}$. The factor B_1/B_2 in (26) is dependent on the transmit pulse shape ($g_{tx}(t)$) used, B_1 is defined as $\max\limits_{r,q}\left\{\sum\limits_{n=0}^{N-1}|g_{tx}([r+qM-nM]_{MN})|^2\right\}$ and B2 is defined as $\frac{1}{MN}\left[\sum\limits_{n=0}^{N-1}\sum\limits_{r=0}^{M-1}\sum\limits_{q=0}^{N-1}|g_{tx}([r+qM-nM]_{MN})|^2\right]$, where $[.]_{MN}$ denotes mod-MN operation. When $g_{tx}(t)$ is rectangular, B_1/B_2 is 1 which results in the upper bound on PAPR for two-step OTFS with rectangular pulse to be

$$\mathrm{PAPR}_{\mathrm{2step,rect}}\leq\frac{N\max\limits_{c\in\mathbb{A}}\{|c|^2\}}{\sigma_a^2}, \tag{27}$$

which is the same as the upper bound obtained for DZT-OTFS with rectangular pulse in (25). However, for non-rectangular

pulses, as we will see in the next section on results and discussions, the PAPR of DZT-OTFS can be better than that of two-step OTFS.

A. CCDF of PAPR

It is important to characterize the PAPR through the CCDF as it gives insight on the probability with which PAPR crosses a certain level γ, i.e, $C_{PAPR}(\gamma) = \Pr(PAPR \geq \gamma)$, where $\Pr(\cdot)$ denotes the probability. For ease of analysis, we consider OTFS system with rectangular transmit pulse. From (1) and (5), it is noted that the time domain transmit sequence is the IFFT of $\mathbf{X}_{DD}$ along the Doppler axis. Also, note that it is assumed that $\mathbf{X}_{DD}[m,k]$ is i.i.d uniform distributed with mean zero and variance σ_s^2. Assume that the modulation alphabet $\mathbb{A}$ is normalized such that $\sigma_s^2 = 1$. Under the above assumptions and noting that IDZT is unitary transformation, if K is large then by central limit theorem, the transmitted complex time domain symbols $x_{td}[w]$ are i.i.d complex Gaussian with mean 0 and variance 1, i.e., $\mathcal{CN}(0,1)$. Then the magnitude of the symbols are Rayleigh distributed and the squared magnitude have exponential distribution with mean 1. Hence,

$$\begin{aligned} C_{PAPR}(\gamma) &= \Pr(PAPR \geq \gamma) \\ &= \Pr(\max_{w\in[0,KL-1]} |x_{td}[w]|^2 \geq \gamma) \\ &= 1 - \Pr(\max_{w\in[0,KL-1]} |x_{td}[w]|^2 < \gamma) \\ &= 1 - \Pr(|x_{td}[0]|^2 < \gamma, \cdots, |x_{td}[KL-1]|^2 < \gamma) \\ &= 1 - (\Pr(|x_{td}[0]|^2 < \gamma), \cdots, \Pr(|x_{td}[KL-1]|^2 < \gamma)) \\ &= 1 - (1-e^{-\gamma})^{KL}. \end{aligned} \tag{28}$$

Equation (28) is the upper bound on the CCDF of PAPR and holds true for the case of Nyquist sampling. Bound on CCDF expression for the case when signal is ovsersampled is obtained as $C_{PAPR}(\gamma) = 1 - (1-e^{-\gamma})^{\alpha KL}$ [14], where α is determined by fitting the analytical CCDF to the simulation results. For sufficiently large K, $\alpha = 2.8$ is a good approximation.

B. PAPR of DZT-OTFS with DD domain indexing

In this subsection, we consider the PAPR performance of DZT-OTFS with two types of DD domain indexing, namely, delay indexing and Doppler indexing as described below.

1) Delay indexing: Here, indexing is done along the delay axis, i.e., I_1 indices out of L delay indices are selected for each of the K Doppler indices, and KI_1 symbols are multiplexed on these selected DD bins. The rate achieved in this indexing scheme is given by

$$\eta_{\text{del}} = \frac{1}{KL}\left(K\left\lfloor \log_2 \binom{L}{I_1} \right\rfloor + KI_1 \log_2|\mathbb{A}|\right) \quad \text{bpcu.} \tag{29}$$

When rectangular transmit pulse is used, $\mathbb{E}\{|\mathbf{x}[m+qL]|^2\} = \sigma_s^2$, $0 \leq q \leq K-1$ and $m \in S_{I_1}$, where S_{I_1} is the set of active delay bins. Thus, the average power in (24) reduces to $I_1\sigma_s^2/L$ and the upper bound on the PAPR of delay indexed DZT-OTFS for rectangular transmit pulse is obtained as

$$\text{PAPR}_{\text{del-dzt,rect}} \leq \frac{KL \max_{a\in\mathbb{A}}\{|a|^2\}}{I_1\sigma_s^2}. \tag{30}$$

2) Doppler indexing: Here, indexing is done along the Doppler axis, i.e., I_2 indices out of K Doppler indices are selected for each of the L delay indices, and LI_2 symbols are multiplexed on these selected DD bins. The achieved rate in this scheme is given by

$$\eta_{\text{dop}} = \frac{1}{KL}\left(L\left\lfloor \log_2 \binom{K}{I_2} \right\rfloor + LI_2 \log_2|\mathbb{A}|\right) \quad \text{bpcu.} \tag{31}$$

When rectangular transmit pulse is used, the upper bound on the numerator of PAPR in (23) becomes $I_2 \max_{a\in\mathbb{A}}\{|a|^2\}$ and hence the upper bound on the PAPR of Doppler indexed DZT-OTFS for rectangular transmit pulse is obtained as

$$\text{PAPR}_{\text{dop-dzt,rect}} \leq \frac{I_2 \max_{a\in\mathbb{A}}\{|a|^2\}}{\sigma_s^2}. \tag{32}$$

Comparing (25) and (32), we can see that PAPR of DZT-OTFS can be improved by Doppler indexing.

IV. Results and Discussions

In this section, we present the simulated PAPR characteristics of DZT-OTFS and compare it with that of two-step OTFS for different pulse shapes. Note that the quantity of interest is the PAPR of the continuous time baseband (CTBS) signal. The PAPR of the discrete time baseband signal (DTBS) $x_{td}[w]$ may not be same as that of PAPR of CTBS $x_{td}(t)$. In practice, measurement of PAPR for CTBS can be done only after implementing the actual hardware. Hence, it is not starightforward. An approximate value of PAPR for CTBS can be obtained using the DTBS if it is Q times oversampled, with $Q \geq 4$, followed by interpolation [15]. In the results presented in the following, both $Q = 1$ and $Q = 4$ are considered based on the significance of each in the context. We also present the PAPR characteristics of DZT-OTFS with indexing and compare with that of two-step OTFS with indexing for non-rectangular pulses.

A. Analytical and simulated CCDF of PAPR for rectangular pulse

Figure 2 shows the simulated CCDF of DZT-OTFS for rectangular pulse with Nyquist sampling, i.e., at sampling instants $t = wT_s/Q$, where $Q = 1$ corresponds to Nyquist sampling and $Q > 1$ corresponds to oversampling. Analytical CCDF is also plotted. In Fig. 2a, an OTFS frame of size $K = 8, L = 256$ is considered. CCDF of PAPR is simulated for different constellation sizes, viz., 4-QAM, 16-QAM, 64-QAM, and 1024-QAM. It is observed that as the constellation size increases, the CCDF moves closer to the analytical bound. In Fig. 2b, the effect of K on PAPR is captured. CCDF of PAPR is obtained for $L = 256$, $K = 4, 64$, and 16-QAM. It is observed that as K increases, the simulated PAPR gets very close to the analytical bound, supporting the concept of Gaussian approximation at large values of K. Also, it is observed that the PAPR increases as a function of K for rectangular pulse.

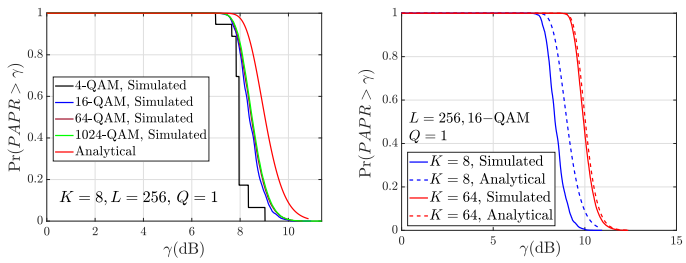

(a) Effect of constellation size on PAPR (b) Effect of K on PAPR

Fig. 2. Analytical and simulated CCDF of the PAPR of DZT-OTFS.

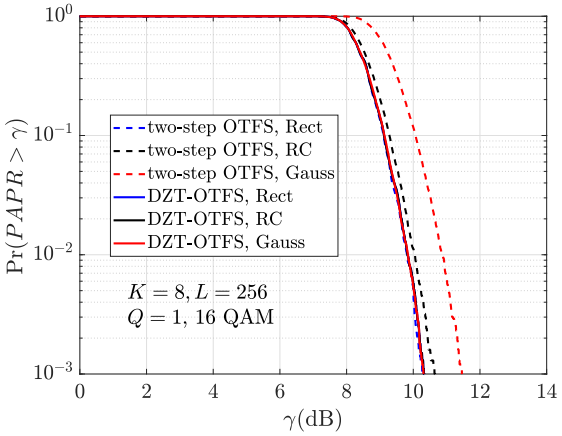

Fig. 3. Comparison of the CCDF of the PAPR of DZT-OTFS and two-step OTFS with Nyquist sampling ($Q = 1$).

B. Comparison of PAPR of DZT-OTFS and two-step OTFS

Figures 3 and 4 show the CCDF plots of the PAPR of DZT-OTFS and two-step OTFS for different transmit pulse shapes with $Q = 1$ and $Q = 4$. System with $K = 8$, $L = 256$, and 16-QAM constellation is considered. Rectangular pulse $p_{tx,rect}(t) = rect(t/T)$, raised cosine pulse $p_{tx,RC}(t) = \frac{\text{sinc}(t/T)\cos(\pi\beta t/T)}{1-4\beta^2(t/T)^2}$, and Gaussian pulse $p_{tx,Gauss}(t) = e^{-\pi\alpha(t/T)^2}$, $-KLT_s/2 \leq t < KLT_s/2$ are considered for studying the effect of pulse shape on PAPR. All pulses are sampled at rate $f_s = 1/T_s$, with $T = T_s$ for DZT-OTFS and $T = LT_s$ for two-step OTFS. The pulses are normalized to have unit energy. To obtain the over-sampled signal, Nyquist sampled signal $x_{td}[w]$ is upsampled by a factor $Q = 4$. The upsampled signal is then reconstructed using a square-root raised cosine FIR filter with roll-off factor 0.5. The FIR filter considered is truncated to span 6 symbol period, with Q samples each. The observations can be summarized as follows. i) CCDF of PAPR with $Q = 4$ has degraded compared to that with $Q = 1$. This is in agreement with the fact that the discrete time baseband signal may not capture all peaks. ii) CCDF of PAPR for DZT-OTFS is superior compared to that of the two-step OTFS for the non-rectangular pulse shapes considered. iii) CCDF of PAPR is almost same for all the pulse shapes in case of DZT-OTFS, whereas CCDF of PAPR of two-step OTFS varies depending on the pulse shape.

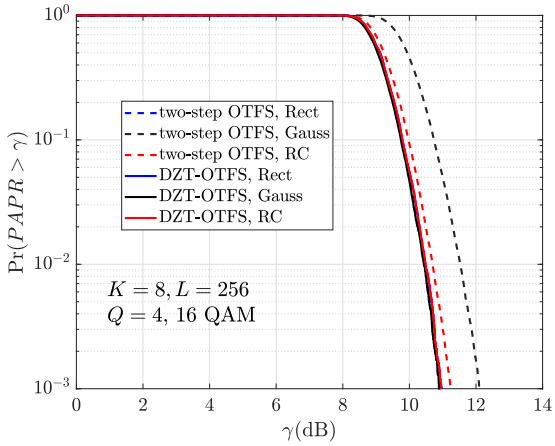

Fig. 4. Comparison of the CCDF of the PAPR of DZT-OTFS and two-step OTFS with over-sampling ($Q = 4$).

C. PAPR of DZT-OTFS with DD domain indexing

Figure 5 shows the simulated CCDF of the PAPR of DZT-OTFS for $K = 8$ and $L = 64$ without indexing, with Doppler indexing ($I_2 = 4$), and with delay indexing ($I_1 = 32$). Rectangular transmit pulse with $Q = 1$ and 4-QAM constellation are considered. We can observe that Doppler indexing improves the PAPR performance while delay indexing worsens the PAPR. Also, the maximum PAPR obtained from simulation for DZT-OTFS without indexing is 9.1 dB, whereas it is 6.3 dB and 12.1 dB with Doppler indexing and delay indexing, respectively, which is roughly in agreement with the upper bounds given by (25), (32), and (30).

Figure 6 shows the simulated CCDF of the PAPR of DZT-OTFS for the same system with Doppler indexing ($I_2 = 2, 4$) and with delay indexing ($I_1 = 16, 32$). We can see the effect of number of active bins on the PAPR performance here. As the number of active Doppler bins (I_2) decreases, the PAPR reduces, which is in agreement with the fact that the PAPR upper bound for Doppler indexed DZT-OTFS depends linearly on I_2. On the other hand, as the number of active delay bins (I_1) decreases, the PAPR increases, which is also in agreement with the fact that the PAPR upper bound for delay indexed DZT-OTFS depends inversely on I_1.

Finally, Fig. 7 shows the simulated CCDF of the PAPR of DZT-OTFS and two-step OTFS for $K = 8$ and $L = 64$ with Doppler indexing ($I_2 = 4$) for RC and Gaussian pulses. It can be seen that with Doppler indexing also, the PAPR performance of DZT-OTFS is superior to two-step OTFS for the considered non-rectangular pulses.

V. Conclusions

PAPR performance of DZT-OTFS was characterized in this paper, which has not been reported before. An upper bound on PAPR of DZT-OTFS for general transmit pulse shapes was derived using Cauchy-Schwartz inequality and a tighter bound was obtained for the case of rectangular pulse. It was shown through analysis and simulation that the PAPR of DZT-OTFS and two-step OTFS are same for rectangular pulse.

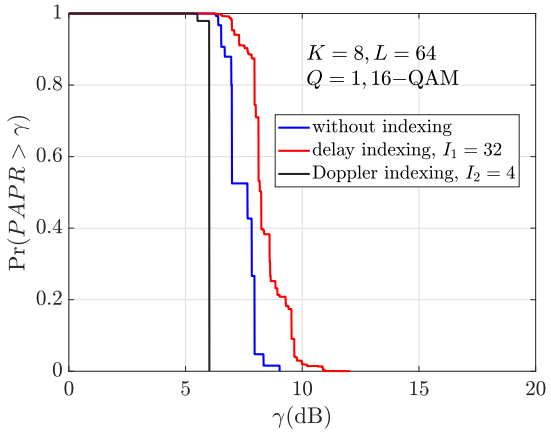

Fig. 5. Comparison of the CCDF of the PAPR of DZT-OTFS with Doppler indexing, delay indexing and without indexing.

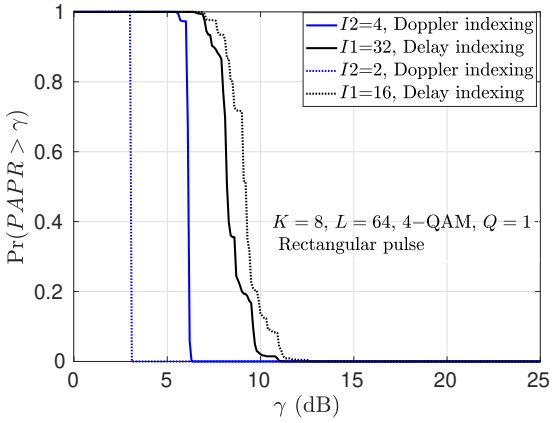

Fig. 6. Effect of the number of active bins on the CCDF of the PAPR of DZT-OTFS with Doppler indexing and delay indexing.

It was observed that for non-rectangular pulses without and with ovsersampling, DZT-OTFS has better PAPR performance compared to two-step OTFS. It was also shown that indexing of DD bins along the Doppler axis can improve the PAPR performance of DZT-OTFS.

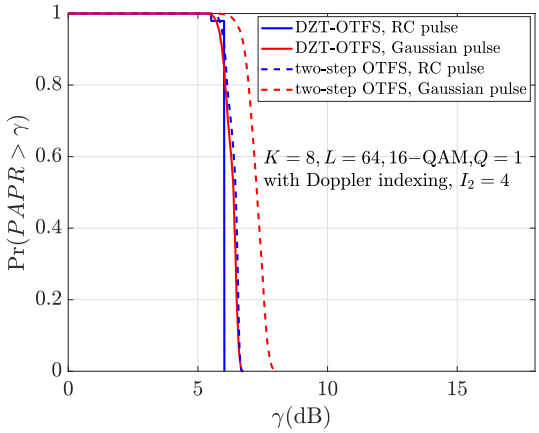

Fig. 7. Comparison of the CCDF of the PAPR of DZT-OTFS and two-step OTFS with Doppler indexing.

REFERENCES

[1] R. Hadani et al., "Orthogonal time frequency space modulation," *Proc. IEEE WCNC'2017*, pp. 1-6, Mar. 2017.

[2] Y. Hong, T. Thaj, and E. Viterbo, *Delay-Doppler Communications: Principles and Applications*, Academic Press, 2022.

[3] A. J. E. M. Janssen, "The Zak transform: a signal transform for sampled time-continuous signals," Philips J. Res., 43, pp. 23-69, 1988.

[4] S. K. Mohammed, "Derivation of OTFS modulation from first principles," *IEEE Trans. Veh. Tech.,* vol. 70, no. 8, pp. 7619-7636, Aug. 2021.

[5] S. K. Mohammed, "Time-domain to delay-Doppler domain conversion of OTFS signals in very high mobility scenarios," *IEEE Trans. Veh. Tech.,* vol. 70, no. 6, pp. 6178-6183, Jun. 2021.

[6] S. K. Mohammed, R. Hadani, A. Chockalingam, and R. Calderbank, "OTFS – a mathematical foundation for communication and radar sensing in the delay-Doppler domain," *IEEE BITS the Information Theory Magazine*, vol. 2, no. 2, pp. 36-55, Nov. 2022.

[7] S. K. Mohammed, R. Hadani, A. Chockalingam, and R. Calderbank, "OTFS – predictability in the delay-Doppler domain and its value in communication and radar sensing," available in https://arxiv.org/abs/2302.08705.

[8] F. Lampel, A. Avarado, and F. M. J. Willems, "On OTFS using the discrete Zak transform," *Proc. IEEE ICC Workshop'2022*, pp. 729-734, May 2022.

[9] T. Thaj, E. Viterbo, and Y. Hong, "General I/O relations and low-complexity universal MRC detection for all OTFS variants," *IEEE Access*, vol. 10, pp. 96026-96037, 2022.

[10] V. Yogesh, V. S. Bhat, S. R. Mattu, and A. Chockalingam, "On the bit error performance of OTFS modulation using discrete Zak transform," *IEEE ICC'2023*, May-Jun. 2023. Also available in https://arxiv.org/abs/2303.12496.

[11] G. D. Surabhi, R. M. Augustine, and A. Chockalingam, "Peak-to-average power ratio of OTFS modulation," *IEEE Commun. Letters*, vol. 23, no. 6, pp. 999-1002, Jun. 2019.

[12] A. J. Goldsmith, *Wireless Communications*. Cambridge, UK: Cambridge University Press, 2005.

[13] S. B. Slimane, "Peak-to-average power ratio reduction of OFDM signals using pulse shaping," *Proc. IEEE GLOBECOM'2000*, pp. 1412-1416 Dec. 2000.

[14] S. B. Slimane, "Reducing the peak-to-average power ratio of OFDM signals through precoding," *IEEE Trans. Veh. Tech.*, vol. 56, no. 2, pp. 686-695, Mar. 2007.

[15] S. H. Han and J. H. Lee, "An overview of peak-to-average power ratio reduction techniques for multicarrier transmission," *IEEE Wireless Communications*, vol. 12, no. 2, pp. 56-65, Apr. 2005.

[16] E. Basar et al., "Index modulation techniques for next-generation wireless networks," *IEEE Access*, vol. 5, pp. 16693-16746, 2017.

[17] Y. Liang, L. Li, P. Fan, and Y. Guan, "Doppler resilient orthogonal time-frequency space (OTFS) systems based on index modulation," *IEEE VTC'2020-Spring*, pp. 1-5, May 2020.

[18] J. K. Francis, R. M. Augustine, and A. Chockalingam, "Diversity and PAPR enhancement in OTFS using indexing," *Proc. IEEE VTC'2021-Spring*, pp. 1-6, Apr. 2021.